Insights into Suction Caisson Installation Utilising the Material Point Method

M. Stapelfeldt[1(✉)], B. Bienen[2], and J. Grabe[1]

[1] Institute of Geotechnical Engineering and Construction Management, Hamburg University of Technology, Harburger Schlossstraße 20, 20179 Hamburg, Germany
marc.stapelfeldt@tuhh.de

[2] Centre for Offshore Foundation Systems, University of Western Australia, M053, Perth, WA 6009, Australia

Abstract. There is an increasing interest to utilise suction caissons as foundations for offshore wind turbines. Significant research has been devoted to developing penetration prediction methods and to understand the in-service response under cyclic loading. However, the effect of the installation process on the state of the surrounding soil is less well understood, although it may affect the in-service performance, in particular under relatively low magnitude cyclic loading, which represents the majority of loading conditions experienced by an offshore wind turbine in the field. This is due to the complexity in modelling the problem, which includes very large deformations, seepage flow and soil-structure interaction. Novel approaches featuring the material point method and centrifuge test results evaluated with the particle image velocimetry post analysis are capable of visualising the mechanisms underlying suction caisson installation. The results aim to reduce existing uncertainties and provide confidence in suction caissons as a reliable foundation system for offshore wind applications.

Keywords: Suction installation · Material point method · Particle image velocimetry

1 Introduction

Suction caissons are increasingly considered to server as foundation systems for offshore wind turbines located at North Sea developments (Tjelta 2015). Suction caissons are circular steel structures, which are equipped with a lid. Suction caissons (also suction called buckets) for offshore wind turbines typically have aspect ratios between $L/D = 0.5$ and $L/D = 1$. L is the skirt length and D is the diameter. The suction caisson installation is performed in two steps: During the first phase, the caisson skirt penetrates into the soil under self-weight. The suction installation commences once a sufficient skirt penetration depth is reach and the caisson movement terminates. The water encapsulated inside the caisson is extracted by means of a pumping system. The resulting internal suction pressure provides additional downforce and yields seepage

M. Barla et al. (Eds.): IACMAG 2021, LNCE 125, pp. 802–809, 2021.
https://doi.org/10.1007/978-3-030-64514-4_86

around the caisson skirt. The seepage flow reduces the skirt tip resistance. The combination of the self-weight, suction pressure and reduced tip resistance enables the caisson installation – even in dese sand (Houlsby and Byrne 2005). However, the seepage flow is expected to modify the soil plug state. particle image velocimetry (PIV) post analysis of centrifuge tests featuring a half-model caisson (Kim et al. 2016; Ragni et al. 2018; Ragni et al. 2019) visualised the effect of suction installation on the state of the sandy soil. Numerical simulations can visualise the underlying mechanisms and provide further insights. Therefore, the material point method (MPM) (Sulsky et al. 1994; Sulsky et al. 1995) is employed here to back-calculate the results obtained from the PIV post analyses results presented in Ragni et al. (2019). In order to do so, the plane strain formulation of the MPM code Anura3D 2019.1 has been extended for axisymmetric analysis as described in Fern et al. (2019).

2 Axisymmetric MPM

The axisymmetric MPM utilises a cylindrical coordinate system, where u_y represents the vertical and u_r is the radial displacement. The strain tensor has got four non-zero components, which are the radial strain ε_r, the vertical strain ε_y, the shear strain γ, and the circumferential strain ε_θ:

$$\varepsilon_r = \frac{\partial u_r}{\partial r}\ \varepsilon_y = \frac{\partial u_y}{\partial y}\ \varepsilon_\theta = \frac{u_r}{r} \tag{1}$$

$$\gamma_{ry} = 2\gamma = \left(\frac{\partial u_r}{\partial y} + \frac{\partial u_y}{\partial r}\right) \tag{2}$$

The distance between the location of a material point (MP) and the axis of symmetry is denoted by the radius r. The strains are linked to displacements through the following equation:

$$\varepsilon = \boldsymbol{B_i u_i} = \begin{Bmatrix} \frac{\partial N_i(x_p)}{\partial r} & 0 \\ 0 & \frac{\partial N_i(x_p)}{\partial y} \\ \frac{\partial N_i(x_p)}{\partial y} & \frac{\partial N_i(x_p)}{\partial r} \\ \frac{\partial N_i(x_p)}{r} & 0 \end{Bmatrix} \boldsymbol{u_i} \tag{3}$$

The matrix $\boldsymbol{B_i}$ is formed by the gradients of the shape functions N, which contain the local coordinates for the MPs x_p. In consequence, the strains in the axisymmetric formulation are given through summation across the element nodes N_n:

$$(\varepsilon_r)_p = \sum_{i=1}^{N_n} u_{r,i} \frac{\partial N_i(x_p)}{\partial r} \tag{4}$$

$$\left(\varepsilon_y\right)_p = \sum_{i=1}^{N_n} u_{y,i} \frac{\partial N_i\left(x_p\right)}{\partial y} \tag{5}$$

$$\left(\varepsilon_\theta\right)_p = \sum_{i=1}^{N_n} u_{r,i} \frac{N_i\left(x_p\right)}{r} \tag{6}$$

$$\gamma_{ry} = \sum_{i=1}^{N_n} \left(u_{y,i} \frac{\partial N_i\left(x_p\right)}{\partial r} + u_{r,i} \frac{\partial N_i\left(x_p\right)}{\partial y} \right) \tag{7}$$

The internal force $\boldsymbol{f_i^{int}}$ is calculated in a specific way in axisymmetric MPM, which is given here:

$$\boldsymbol{f_i^{int}} = \sum_{p=1}^{N_p} \boldsymbol{B_i^T}\left(x_p\right) \boldsymbol{\sigma_p} \Omega_p \tag{8}$$

N_p represents the number of MPs which are located inside an element in the beginning of a time step. Ω_p is the integration weight of a MP and $\boldsymbol{\sigma_p}$ is the related stress tensor. The radial and vertical components are given in the following equations:

$$f_{r,i}^{int} = \sum_{p=1}^{N_p} \left\{ \left(\left(\sigma_r\right)_p \frac{\partial N_i\left(x_p\right)}{\partial r} + \left(\sigma_{ry}\right)_p \frac{\partial N_i\left(x_p\right)}{\partial y} + \left(\sigma_{\theta\theta}\right)_p \frac{\partial N_i\left(x_p\right)}{r} \right) \Omega_p \right\} \tag{9}$$

$$f_{y,i}^{int} = \sum_{p=1}^{N_p} \left\{ \left(\left(\sigma_y\right)_p \frac{\partial N_i\left(x_p\right)}{\partial y} + \left(\sigma_{ry}\right)_p \frac{\partial N_i\left(x_p\right)}{\partial r} \right) \Omega_p \right\} \tag{10}$$

Despite the presented differences, the calculation scheme of the axisymmetric formulation is similar to the procedure for a conventional plane-strain MPM, which is also presented in detail in Fern et al. (2019).

3 Numerical Model

The MPM analyses aim to visualise the mechanisms underlying the suction caisson installation. This study features a comparison to the centrifuge test results presented in Ragni et al. (2019) in order to validate the numerical model. The numerical simulations are performed with a modified version of the MPM code Anura3D 2019.1. The modifications discussed in Sect. 2 enable the simulations of the skirt penetration with frictional soil-structure interaction while seepage flow around the skirt tip is present.

The numerical model shown in Fig. 1 features the caisson that is pre-embedded in the soil. The dimensions, shown in Fig. 1a were derived under consideration of the centrifuge tests and were also found to minimise boundary effects. The two-dimensional axisymmetric model consists of triangular elements containing three MPs

each in the beginning of the analysis. The mesh shown in Fig. 1b illustrates that small elements are located close to the caisson. A coarser mesh is utilised further away from the area where the largest deformations are expected. The caisson diameter is $D = 5$ m, the skirt length is $L = 5$ m and the wall thickness is $t = 5$ cm in prototype scale.

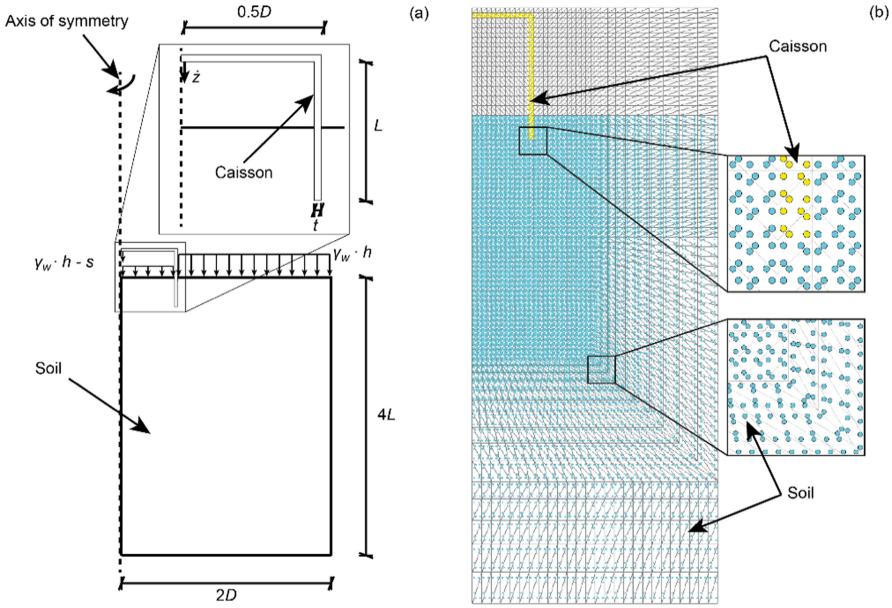

Fig. 1. Dimensions (a) and discretization (b) of the numerical model utilised for MPM analyses of the suction caisson installation in a uniform sand profile

Horizontal displacements are prevented at the axis of symmetry and outside vertical edge of the model geometry, while vertical displacements are permitted. The bottom features zero vertical displacements boundary conditions. These three edges are also hydraulically impermeable. The displacements at the soil surface are free, while solid and liquid pressure boundary conditions are applied on the MPs as shown in Fig. 1a in order to establish the differential pressure. The caisson is modelled as a quasi-rigid body as the horizontal displacement rate is $\dot{z}_h = 0$ and a prescribed vertical displacement rate $\dot{z}_v$ is utilised to control the caisson penetration.

The (jacked) self-weight penetration in the centrifuge test was performed slowly and in a controlled fashion, as it is executed in the field. This is assumed to result in drained conditions. Hence, it was possible to model the soil as a drained one-phase continuum for the jacked penetration. The course of the suction installation is determined by the pore pressure regime. Thus, a *v-w*-formulation is required for the simulations of the suction installation. The state variables for the soil and the liquid phase are stored in the same MP – i.e. the one martial point, two-phase MPM is employed. The mixed integration scheme is utilised in order to minimise numerical errors due to

grid crossing, which can result in artificial stress and pore pressure oscillations (Jassim et al. 2013 and Fern et al. 2019).

The elastic-plastic constitutive model featuring the Mohr-Coulomb plasticity criterion is utilised. The model parameters summarised in Table 1 are determined under consideration of laboratory test results summarised in Tran (2005), Lehane et al. (2013), and Chow et al. (2018). A reduced liquid bulk modulus is utilised in order to reduce computational costs. The value given in Table 1 is a minimum value that avoids a major influence on the results (Fern et al. 2019). The initial porosity n and the interface friction coefficient $\mu = 0.15$ are derived from the results of the centrifuge experiments discussed in Ragni et al. (2018) and Ragni et al. (2019).

Table 1. Model parameters for MPM simulations featuring fine silica sand.

Parameter	Symbol	Unit	Fine silica sand
Friction angle	φ	(°)	38
Dilatancy angle	ψ	(°)	1
Effective cohesion	c	(kPa)	0
Young's modulus	E	(MPa)	60
Poisson's ratio	ν	(-)	0.25
Intrinsic permeability	κ	(m^2)	$1 \cdot 10^{-11}$
Dynamic viscosity liquid	η_w	(kPa · s)	$1 \cdot 10^{-6}$
Bulk modulus liquid	K_w	(kPa)	20000
Density water	ρ_w	(t/m^3)	1
Initial porosity	n	(-)	0.35
Grain density solid	ρ_s	(t/m^3)	2.65

The simulations are conducted according to the following procedure: First, the effective stresses and, if necessary the hydrostatic pressure, are applied during the K_0 procedure. The caisson is penetrated displacement controlled in a second step.

The caisson penetration rate $\dot{z}_v$ and the internal suction pressure s are estimated under consideration of the fast caisson penetration of Test 3 (Ragni et al. 2019). The penetration rate in the numerical model is assumed to decrease linearly with ongoing caisson depth from $\dot{z}_v = 0.2$ m/s to $\dot{z}_v = 0.08$ m/s. The differential pressure is applied simultaneously, if required. This differential (or suction) pressure is calculated following the procedure presented in Houlsby and Byrne (2005) and using the parameters given in Ragni et al. (2019). A ratio of internal to external effective permeabilities $k_i/k_o = 1$ has previously been found to agree well with measurements from centrifuge tests (Bienen et al. 2018). The development of the normalised suction pressure from the prediction of Test 3 (Ragni et al. 2019) is considered: The applied normalised suction pressure starts at $s/(\gamma' D) = 0$ and increases preeningly linear towards $s/(\gamma' D) = 1$ at a relative penetration depth of $\Delta z/L = 1$. The suction pressure is normalised by the effective specific density of the sand $\gamma' = 10.5$ kN/m^3 and the caisson diameter $D = 5$ m.

4 Results and Discussion

The simulated suction caisson installation is compared with experimental results obtained from PIV analyses to ensure that the MPM model captures the relevant mechanisms. The presented displacements are normalised by the considered vertical caisson displacement Δz as referred in Ragni et al. (2018). Figure 2 compares the calculated results of a jacked caisson installation to the corresponding experimental data pretend in Ragni et al. (2019). The calculated results on the right-hand side (RHS) of Fig. 2 show a separated mechanism at shallow penetration depths, which is similar to the experiments shown on the left-hand side (LHS) of Fig. 2. A combined mechanism indicating plug heave has formed at a penetration depth of $z/L = 0.3$ in the experimental and the numerical results. Furthermore, symmetrically soil displacement at the skirt tip is evident in the experiment and in the numerical simulation. Hence, the numerical model is considered to be suitable for the simulation of the jacked caisson installation.

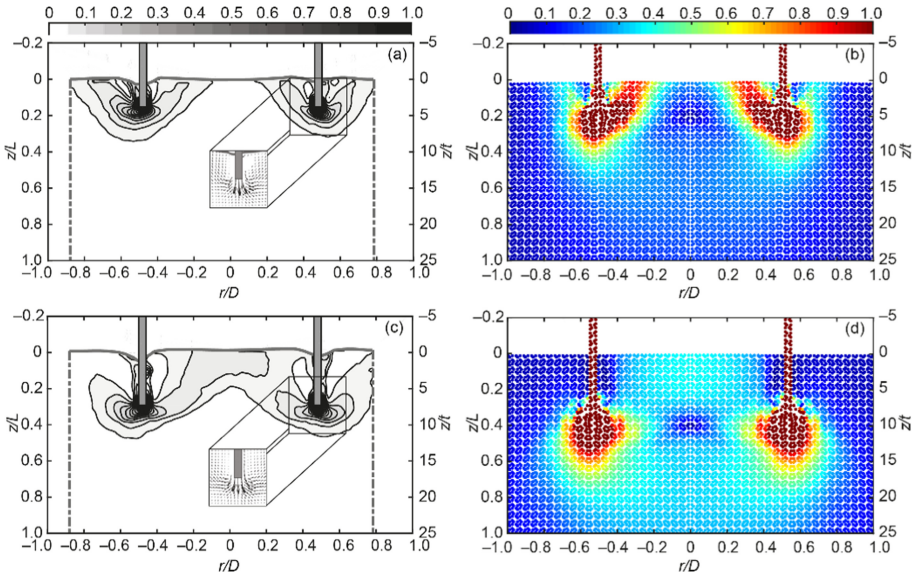

Fig. 2. Comparison of normalised resultant displacements during the self-weight penetration in dense sand obtained from PIV analyses (LHS, Ragni et al. 2019) and axisymmetric MPM analyses (RHS) at increasing normalised penetration depths z/L = 0.15 (a, b); z/L = 0.30 (c, d).

The calculated results of the suction installation phase presented in Fig. 3 feature the same inverted V-shaped mechanism that was observed by Ragni et al. (2019). The resultant displacements show minor downward movement of the soil outside the caisson skirt due to the frictional interaction. Upward displacement is observed inside the caisson. The largest heave occurs in the centre of the caisson. The internal frictional

interaction reduces the heave close to the skirt. This behaviour is similar to the experimental results, albeit Fig. 3d shows only minor uplift.

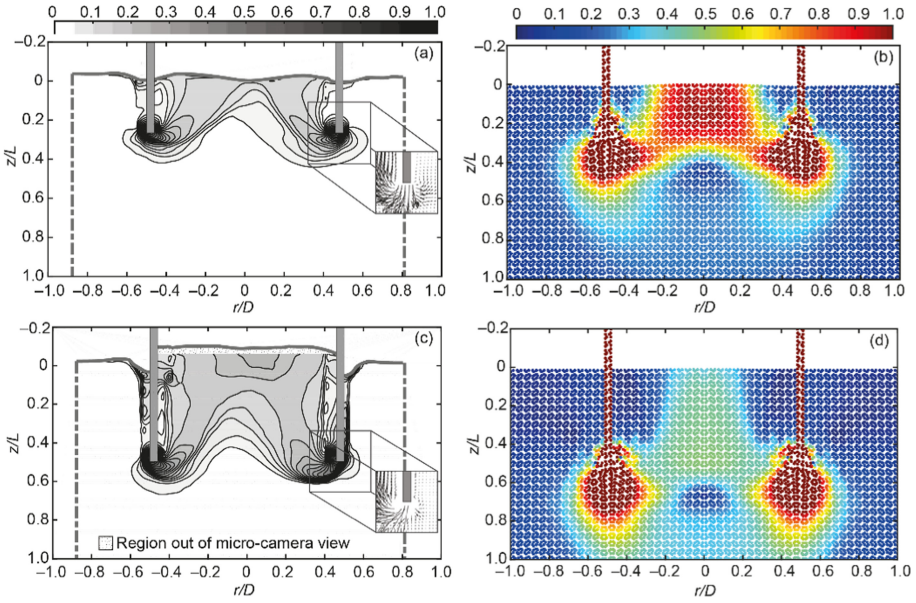

Fig. 3. Comparison of normalised resultant displacements during the suction installation in dense sand obtained from PIV analysis (LHS, Ragni et al. 2019) and axisymmetric MPM analyses (RHS) at increasing normalised penetration depths z/L = 0.28 (a, b); z/L = 0.51 (c, d).

The simulations of the suction installation had to be re-started at a certain penetration depth, which is analogue to the PIV post analyses that were also conducted stepwise (Ragni et al. 2019). Hence, the accumulation of the plug heave and therefore the upward movement of the internal soil surface differ, but the resultant displacement contours are comparable. Consequently, it is demonstrated that the presented numerical model is suitable for the simulation of the suction caisson installation in saturated sand.

5 Concluding Remarks

An MPM model capable of the simulation of the self-weight and suction installation of a caisson foundation into sand is established. The numerical model, validated through the comparison with centrifuge test results, visualises the underlying mechanisms. The presented numerical model is expected to facilitate further investigation of the suction caisson installation and the response to monotonic and repetitive loading.

Acknowledgements. We acknowledge the support from the Deutsche Forschungsgemeinschaft (DFG) for our research project GR 1024/26-2 Sauginstallation Maritimer Strukturen (SIMS). We acknowledge the support of Alexander Rohe (Deltares) and the Anura3D MPM research

community. This work forms part of the activities of the Centre for Offshore Foundation Systems (COFS), which is currently supported as a Centre of Excellence by the Lloyd's Register Foundation. Lloyd's Register Foundation helps to protect life and property by supporting engineering-related education, public engagement and the application of research. This support is gratefully acknowledged.

References

Bienen, B., Klinkvort, R.T., O'Loughlin, C.D., Zhu, F., Byrne, B.W.: Suction caissons in dense sand, part I: installation, limiting capacity and drainage. Géotechnique **68**(11), 937–952 (2018). https://doi.org/10.1680/jgeot.16.P.281

Chow, S.H., O'Loughlin, C.D., Gaudin, C., Lieng, J.T.: Drained monotonic and cyclic capacity of a dynamically installed plate anchor in sand. Ocean Eng. **148**, 588–601 (2018). https://doi.org/10.1016/j.oceaneng.2017.11.051

Fern, E.J., Rohe, A., Soga, K., Alonso, E.: Material Point Method for Geotechnical Engineering: A Practical Guide. CRC Press, Boca Raton (2019)

Houlsby, G.T., Byrne, B.W.: Design procedures for installation of suction caissons in sand. Geotech. Eng. **158**(3), 135–144 (2005). https://doi.org/10.1680/geng.158.3.135.66297

Jassim, I., Stolle, D., Vermeer, P.: Two-phase dynamic analysis by material point method. Int. J. Numer. Anal. Meth. Geomech. **37**(15), 2502–2522 (2013). https://doi.org/10.1002/nag.2146

Kim, D.-S., Lee, S.-T., Kim, J.-H.: Centrifuge model tests on installation of suction caissons in sand. In: The 6th Japan-Korea Geotechnical Workshop, pp. 73–77 (2016). https://doi.org/10.3208/jgssp.v04.k05

Lehane, B.M., Liu, Q.B.: Measurement of shearing characteristics of granular materials at low stress levels in a shear box. Geotech. Geol. Eng. **31**(1), 329–336 (2013). https://doi.org/10.1007/s10706-012-9571-9

Ragni, R., Bienen, B., Stanier, S.A., Cassidy, M.J, O'Loughlin C.D.: Visualisation of mechanisms governing suction bucket installation in dense sand. In: Physical Modelling in Geotechnics, vol. 1, pp. 651–565. CRC Press (2018)

Ragni, R., Bienen, B., O'Loughlin, C.D., Stanier, S.A., Cassidy, M.J.: Observations during suction bucket installation in sand. Int. J. Phys. Model. Geotech., 1–49 (2019). https://doi.org/10.1680/jphmg.18.00071

Sulsky, D., Chen, Z., Schreyer, H.L.: A particle method for history-dependent materials. Comput. Meth. Appl. Mech. Eng. **118**(1–2), 179–196 (1994)

Sulsky, D., Zhou, S.-J., Schreyer, H.L.: Application of a particle-in-cell method to solid mechanics. Comput. Phys. Commun. **87**(1–2), 236–252 (1995)

Tjelta, T.I.: The suction foundation technology. In: Meyer, V. (ed.) Frontiers in Offshore Geotechnics III, pp. 85–93. Balkema, Leiden (2015). https://doi.org/10.1201/b18442-6

Tran, M.N.: Installation of Suction Caissons in Dense Sand and the Influence of Silt and Cemented Layers. Ph.D. thesis. The University of Sydney, Sydney (2005)